PCCP
Physical Chemistry Chemical Physics

Accepted Manuscript

This article can be cited before page numbers have been issued, to do this please use: A. Kocot, B. A. Nikiel, J. Karcz and P. Kula, *Phys. Chem. Chem. Phys.*, 2026, DOI: 10.1039/D6CP00046K.

This is an Accepted Manuscript, which has been through the Royal Society of Chemistry peer review process and has been accepted for publication.

Accepted Manuscripts are published online shortly after acceptance, before technical editing, formatting and proof reading. Using this free service, authors can make their results available to the community, in citable form, before we publish the edited article. We will replace this Accepted Manuscript with the edited and formatted Advance Article as soon as it is available.

You can find more information about Accepted Manuscripts in the Information for Authors.

Please note that technical editing may introduce minor changes to the text and/or graphics, which may alter content. The journal's standard Terms & Conditions and the Ethical guidelines still apply. In no event shall the Royal Society of Chemistry be held responsible for any errors or omissions in this Accepted Manuscript or any consequences arising from the use of any information it contains.

ROYAL SOCIETY OF CHEMISTRY

rsc.li/pccp

View Article Online
DOI: 10.1039/D6CP00046K

Molecular Organization in Polar Nematic Phases: A Combined FTIR Spectroscopy and Molecular Simulation Approach

Antoni Kocot[1]*, Bartosz Nikiel[1], Jakub Karcz[2] and Przemysław Kula[2]
[1]Institute of Materials Engineering, Faculty of Science and Technology, University of Silesia, Chorzów, Poland;
[2]Institute of Chemistry, Faculty of Advanced Technologies and Chemistry, Military University of Technology, Warsaw, Poland;
* *Corresponding author's e-mail:*

Abstract

The emergence of polar nematic phases, such as the ferroelectric (N_F) and antiferroelectric (N_X) phases, has opened new frontiers in soft matter science. However, the relationship between molecular structure, intermolecular interactions, and the resulting macroscopic order remains poorly understood. This work investigates the molecular organization in the polar nematic phases of the nJK (n=1-5) homologous series using a combined approach of polarized Fourier-Transform Infrared (FTIR) Spectroscopy, Density Functional Theory (DFT) calculations, and Atomistic Molecular Dynamics (MD) Simulations.

A central finding is the inadequacy of single-molecule DFT models to describe the system. While DFT accurately predicts vibrational band positions, it fails to replicate their experimental intensities, suggesting that intermolecular interactions are dominant. This is further corroborated by the anomalous temperature dependence of the average absorbance for parallel and perpendicular vibrations, which deviates significantly from simple density effects. Atomistic MD simulations of a multi-molecule system provide insight into this behavior, revealing the formation of locally ordered nanodomains driven by strong short-range correlations. Experimentally, we quantified the primary nematic order parameter (S), which follows a typical progression in the N phase but shows anomalous changes at the N-N_X and N_X-N_F transitions, ultimately saturating at a high value of $S \approx 0.7$ in the ferroelectric state. The difference between orthogonal absorbance components for perpendicular vibrations reveals a significant biaxiality order parameter (C) that increases upon cooling and exceeds 1 in the N_F phase. This study demonstrates that the unique properties of polar nematics are governed by specific molecular self-assembly and establishes phase biaxiality as a key feature of these systems.

I. Introduction

Polar liquid crystalline (LC) materials have become a subject of renewed scientific interest since they were found to exhibit novel polar nematic phases, such as the ferroelectric (N_F) and antiferroelectric (N_X) phases. Over a century after Max Born's original idea [1], experimental groups from UK and Japan have announced pioneering discoveries in the field of polar nematics. The compounds are referred to as RM734 [2] and DIO [3] and were shown to exhibit the N_F phase [4] in which the director does not possess inversion symmetry, and the phase is polar. The N_F phase has huge application potential and underpinning this are properties including high polarisation values [2, 3, 5, 6], strong non-linear optical response [7-11], large

dielectric permittivities [12-20] and switching at very low electric fields [2, 3, 21–26]. Recently, the first example of a compound with an enantiotropic N_F phase, based on the DIO molecule, was reported. Further modification of the chemical structure DIO molecule led to the discovery of a new chiral LC phase in which polar order coexists with the spontaneous formation of a helical superstructure from achiral molecules [11].

As polar soft materials, phases like N_{TB}, N_{SB}, N_S, and N_F possess the potential to transform future technologies, for instance, in ultra-fast, energy-saving flexible displays, non-volatile memory, and supercapacitors. Consequently, the N_F phase has become an extremely "hot" research topic, attracting leading teams from the US, EU, Japan, and China.

However, the self-organization mechanisms in these new nematic phases are still poorly understood. Our goal is to contribute to this research by developing mesoscopic and microscopic models that correlate experimental observations with molecular characteristics, local N_F symmetry, and macroscopic properties. Current experiments suggest that the stabilization of the phase may be related to a strong softening of one of the Frank elastic constants in the adjacent conventional nematic (N) phase. This softening appears to depend on molecular shape through packing entropy and the correlation of molecular dipoles.

We aim to investigate this hypothesis, particularly to understand why highly fluorinated molecules with strong dipole moments, such as nJK, favour a ferroelectric order over the energetically more favourable anti-parallel correlations in the liquid state. The emerging field of ferroelectric nematic liquid crystals marks an exciting stage in soft matter science. The fluid nature of the N_F phase presents unique challenges and opportunities. Unlike in solid ferroelectrics, where polarization is anchored to the crystal lattice, the polarization vector in a fluid nematic can be continuously deformed, for example, through surface patterning [27, 28] or applied electromagnetic fields. This offers potential for superior spatiotemporal control.

To elucidate the relationship between molecular structure and macroscopic properties in these polar nematic phases, vibrational spectroscopy is a powerful tool. For an anisotropic system, it can provide information about the orientational order of individual functional groups and their specific interactions. In this work, we use polarized Fourier-transform infrared (FTIR) spectroscopy to study the molecular orientational arrangement in the nematic phases (N, N_X, N_F,) of material series: nJK (where n=1-5).

II. Materials and Methods

2.1. Materials

The liquid crystal samples, nJK (n=1-5), were synthesized by the Liquid Crystal Group at the Military University of Technology. Their phase transition temperatures and enthalpies (in brackets, kJ/mol) are as follows [15]:

- **1JK:** Iso 107.4°C [4.47] N_F 78.4°C [23.67] Cr
- **2JK:** Iso 92.4°C [2.86] N_F 67.6°C [19.33] Cr1 55.0°C [1.39] Cr2
- **3JK:** Iso 115.7°C [0.69] N 90.9°C [0.01] N_X 86.8°C [0.38] N_F 65.9°C [20.16] Cr
- **4JK:** Iso 113.0°C [0.55] N 77.0°C [0.007] N_X 68.7°C [0.32] N_F 59.1°C [21.30] Cr

View Article Online
DOI: 10.1039/D6CP00046K

- **5JK:** Iso 115.5°C [0.5] N [17.58] 59.5°C Cr

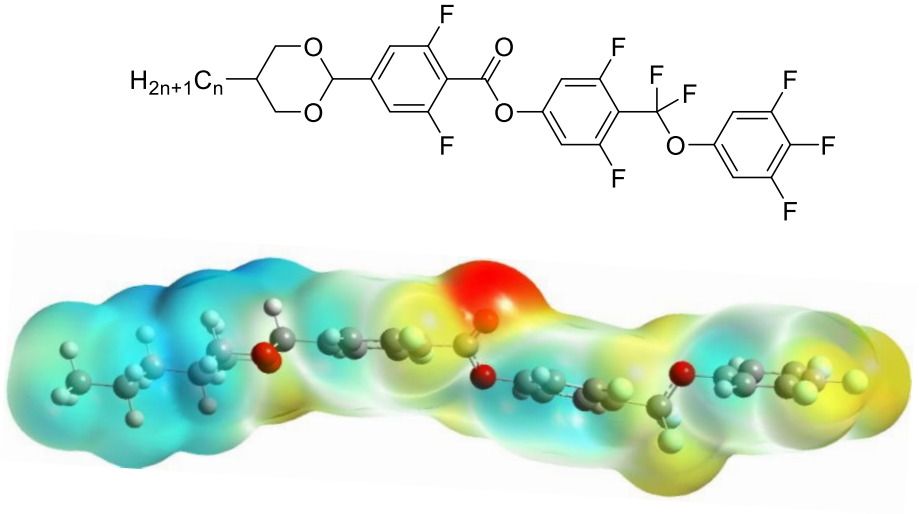

Figure 1. General structure of investigated materials with its electrostatic isopotential surface, highlighting the charge distribution along the molecule.

2.2. Sample Preparation and Alignment

Samples for IR studies were prepared in cells made from two optically polished zinc selenide (ZnSe) windows. To achieve homogeneous planar alignment, the inner surfaces of the windows were spin-coated with the commercial polymer aligning agent SE-130 (Nissan Chemical Industries, Ltd.). The windows were assembled with rubbing directions parallel to each other. Mylar foil was used as a spacer, and the cell thickness was determined to be between 5.0 and 8.0 µm by analyzing interference fringes with an Avaspec-2048 spectrometer. The cells were filled by capillary action in the nematic phase, approximately 5 K below the transition to the isotropic phase. The quality of the alignment was confirmed using an Olympus BX56 polarizing microscope.

2.3. FTIR Spectroscopy

Infrared absorbance measurements were carried out using a Bruker INVENIO FTIR spectrometer equipped with a Hyperion II infrared microscope. An IR-KRS5 grid polarizer was used to polarize the IR beam. Spectra were recorded in the 500–4000 cm^{-1} range with a resolution of 2 cm^{-1}. To improve the signal-to-noise ratio, 32 scans were averaged for each measurement. The sample temperature was controlled by a PID controller with an accuracy of ±0.002 K, and measurements were performed during slow cooling and heating cycles at a rate of 0.5 K/min.

2.4. Theoretical Framework and Order Parameter Calculation

For an anisotropic system, the IR absorbance of the i-th vibrational mode [21] is proportional to the square of the derivative of the system's dipole moment with respect to the normal coordinate, Qi. :

$$A_i = \int_{\nu 1}^{\nu 2} A(\nu)\,d\nu = \frac{N\pi}{3c}\left[\frac{d\mu_i}{dQ_i}\right]^2 \qquad (1)$$

where: N is the number of molecules per unit volume, μ is the molecule dipole moment, and Q_i is the normal coordinate corresponding to the i_{th} mode.

View Article Online
DOI: 10.1039/D6CP00046K

The absorbance components measured in the laboratory frame (X, Y, Z) are related to the molecular orientational order parameters [22, 23] by the following equations:

$$A_X/A_0 = 1 + (S-P)(3/2\,sin^2\,\beta - 1) + 1/2(D-C)(sin^2\,\beta\,cos\,2\,\varphi)$$
$$A_Y/A_0 = 1 + (S+P)(3/2\,sin^2\,\beta - 1) + 1/2(D+C)(sin^2\,\beta\,cos\,2\,\varphi)$$
$$A_Z/A_0 = 1 + S(2 - 3\,sin^2\,\beta) - D\,sin^2\,\beta\,cos\,2\,\varphi \qquad (2)$$

where $A_0 = (A_X+A_Y+A_Z)/3$ is the average absorbance. β and φ are the polar and azimuthal angles of the transition dipole moment in the molecular frame, respectively. *S* and *D,* are the long molecular axis orientational and molecular biaxiality order parameters, while *P* and *C* describe the phase biaxiality.

2.5. Computational Methods

To support the interpretation of experimental spectra, Density Functional Theory (DFT) calculations and atomistic molecular dynamics (MD) simulations were performed. DFT was used to analyze molecular conformations, determine rotational energy barriers, and calculate vibrational spectra for isolated molecules [24]. MD simulations of a system containing 576 molecules of 3JK (Scheme S1) were used to investigate the influence of the local environment and intermolecular interactions on the system's properties, with a primary qualitative focus on molecular packing and orientational ordering processes. Molecular dynamics simulations were performed using GROMACS 2024.3 [27], compiled with EasyBuild 4.9.4 and linked against PLUMED 2.9.2, on the ARES supercomputer at AGH Cyfronet, Kraków.

Intermolecular interactions were described using a modified version of the General Amber Force Field (GAFF) [29]. To better reproduce the conformational flexibility of the liquid-crystalline molecule, dihedral potentials for key torsions were refined following the Liquid Crystal Force Field (LCFF) methodology introduced by Wilson et al. [25]. Specifically, while the validated LCFF Ryckaert–Bellemans parameters were adopted for the flexible alkyl tails, custom torsional potentials were explicitly derived for the unique conjugated linkages within the mesogenic core (e.g., ester and ether bridges). This was achieved by performing relaxed Potential Energy Surface (PES) scans at the B3LYP/6-311+G(d,p) GD3BJ level of theory (Fig. S1). To isolate the pure torsional energy, the classical molecular mechanics background was subtracted from the quantum mechanical profiles, and the resulting target energies were fitted to the Ryckaert–Bellemans polynomial function (Table S1 and S2). Molecular topologies were generated with the ACPYPE server [30]. Atomic partial charges were derived from the electrostatic potential (ESP) using the Merz-Kollman (MK) scheme, as implemented in Gaussian 16 [24]. These quantum-chemically derived charges were used directly without empirical rescaling to provide a more accurate representation of the molecule's specific electronic distribution.

The simulation system consisted of 576 molecules, arranged in an initial nematic order as an apolar 1:1 mixture of molecules aligned along +x and –x [28]. To fully capture high-frequency intramolecular vibrations, no bond length constraints were applied (constraints = none), and the equations of motion were integrated with a time step of 1 fs (0.001 ps). The initial configuration was relaxed for 100 ns at a starting temperature of 340 K, leading to an equilibrated density of approximately 1.3 g·cm^{-3}. Subsequently, the system was heated in a stepwise manner with a temperature increment of 5 K. All simulations were carried out under periodic boundary conditions in all three spatial dimensions. Temperature control was achieved

View Article Online
DOI: 10.1039/D6CP00046K

using a velocity-rescale thermostat [26], while pressure was maintained at 1 bar using an anisotropic Parrinello–Rahman barostat [31], allowing independent fluctuations of the simulation box dimensions. Long-range electrostatic interactions were treated using the Particle Mesh Ewald (PME) method [34] with a real-space cut-off of 1.2 nm. The same cut-off distance was applied to van der Waals interactions.

The influence of temperature on the structural properties of the system was investigated in the range 340–420 K. For each temperature step, the system was equilibrated for 100 ns, followed by an additional 300 ns production run for data collection. The achievement of equilibrium prior to the production runs was verified by confirming that thermodynamic observables (potential energy, temperature, and mass density) had reached stable plateau values without long-term drift. Furthermore, structural convergence was verified by monitoring the time evolution of the orientational order parameters P_2 and P_1. While it is acknowledged that full translational diffusion in low-temperature, highly ordered phases (e.g., the N_F phase) is exceptionally slow, the 100 ns timescale proved fully sufficient to achieve stable orientational ordering for our qualitative analysis**.**

The primary objective of the simulations was to analyze the temperature dependence of these orientational order parameters. The analysis was performed using a custom Python script utilizing the MDAnalysis library [32, 33]. The nematic order parameter, P_2 was determined by diagonalizing the Saupe ordering tensor, Q, constructed from the molecular long axes (defined as the principal axis of the smallest moment of inertia). The phase director, n, corresponds to the principal eigenvector of Q. The polar order parameter P_1 was calculated as the ensemble average of the projection of the normalized molecular dipole moment vectors onto the phase director, n. This comprehensive analysis enabled the characterization of changes in the degree of molecular ordering as a function of temperature.

III. Results and Discussion

3.1. Vibrational Band Assignment and Challenges of DFT Modeling

The complex structure of the studied molecules necessitates a detailed analysis of their possible conformations. DFT calculations were performed to identify low-energy conformers and simulate their corresponding IR spectra. Several energetically stable conformations were found, differing mainly by the torsional angles (φ1-φ5) in the molecular core. The energy barriers between these conformers are comparable to the thermal energy (kT), suggesting that multiple conformations coexist in the condensed phases.

View Article Online
DOI: 10.1039/D6CP00046K

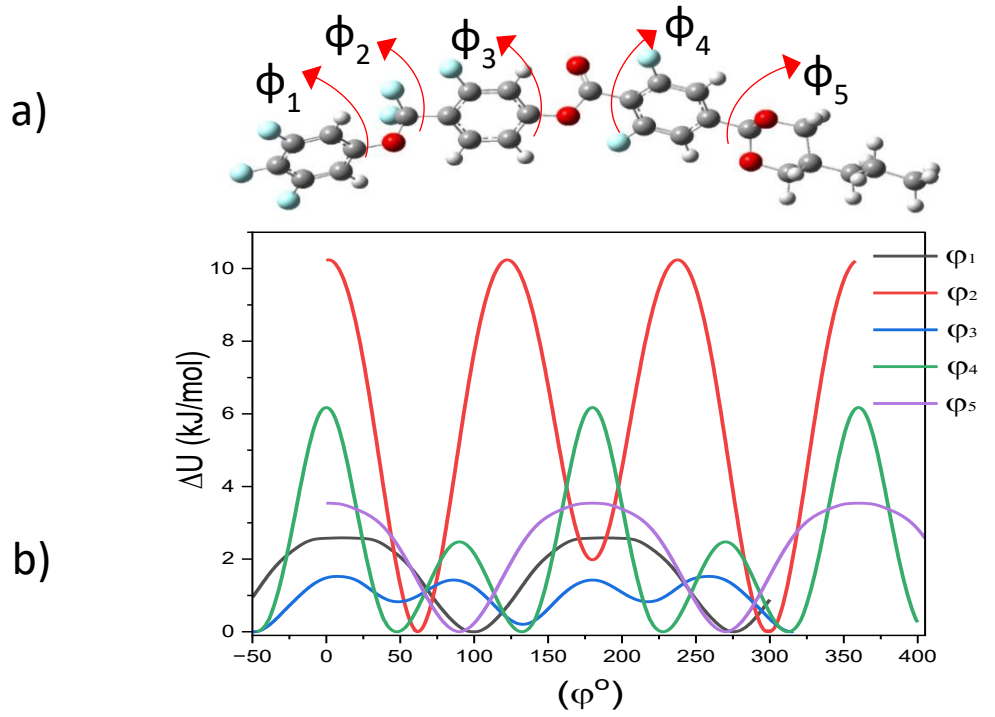

Figure 2. a) Definition of the investigated dihedral angles of the 3JK molecule. b) The calculated potential energy functions for the torsional motion of 3JK molecule relative to the minimum value; black solid line—ϕ1, red solid line— ϕ2, , blue solid line—ϕ3. green solid line—ϕ4, , violet solid line—ϕ5.

A comparison of the calculated spectra with experimental data reveals a significant challenge, fig 3. While DFT simulations can accurately predict the positions of the main vibrational bands, they fail to reproduce their relative intensities.

Specifically, for isolated molecules, the calculated intensities of parallel bands (vibrations with transition dipoles aligned with the long molecular axis) are much higher than observed experimentally, while the intensities of perpendicular bands are lower. This discrepancy points to the crucial role of the intermolecular environment, which is neglected in calculations for a single molecule.

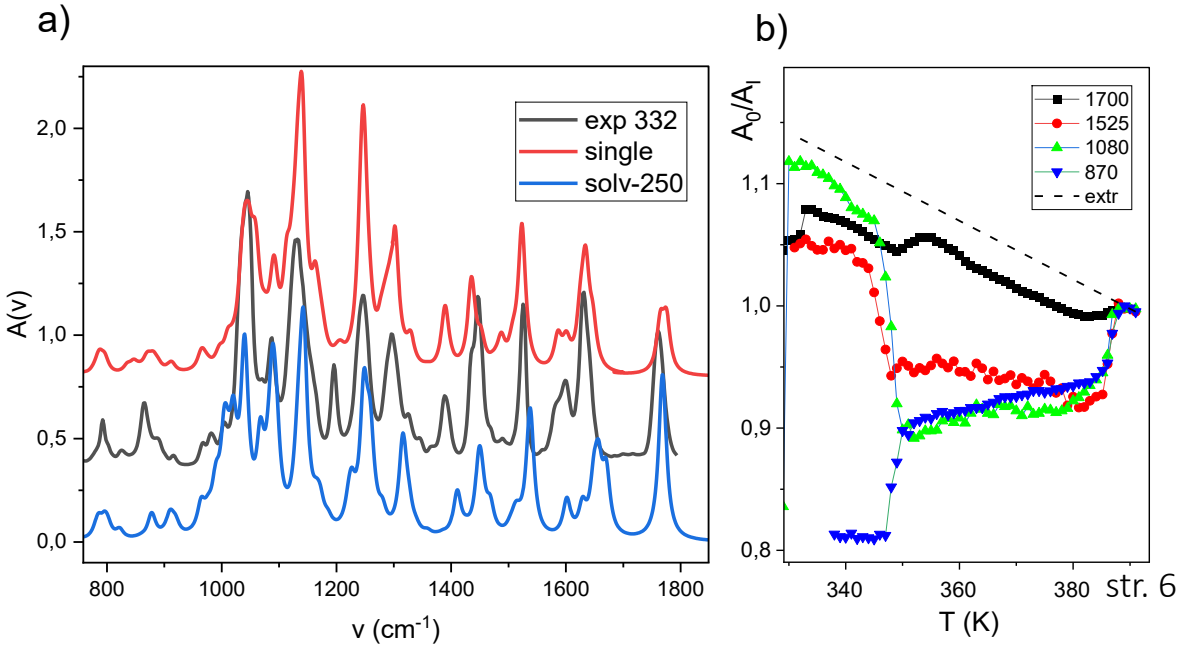

View Article Online
DOI: 10.1039/D6CP00046K

Figure 3. a) The comparison of the experimental spectrum (332 K) with the theoretical spectra (B3-LYP/6-311G+ (d,p)) for the 3JK molecule. Top curve – DFT simulated spectra of single molecule- red solid line, middle curve – experimental spectra - black solid line, bottom curve – DFT calculated spectra of single molecule in the solvent (eps=250) - blue solid line. b) temperature dependence of the average absorbance for parallel and perpendicular vibrations

Attempts to account for the environment by modeling the molecule in a solvent with high dielectric permittivity (ε=30÷300), that corresponds the permittivity in the nematic range. This improved the intensity ratios but worsened the agreement of band positions and spectral shapes. This simplistic approach fails to capture the anisotropic nature of the liquid crystalline environment.

3.2. Role of Intermolecular Interactions and Local Ordering

To more realistically model the influence of the environment, we performed atomistic MD simulations for a system of 576 3JK molecules. Visualizations of the simulation snapshots reveal the formation of small, locally ordered nanodomains with correlated molecular orientations. These domains grow in size as the temperature is lowered Fig 4.b). They show Intrinsic Relaxor-Like Nature in Polar Nematic LC [28].

The long-range dipole-dipole interaction can be described by an anisotropic Kirkwood coefficient, g, which is a measure how the dielectric strength increases with respect to the system of defined as the corresponding dipole correlation functions G(r).

$$g = 1 + V^{-1} \int G\,(r) dr \qquad G(r) = \frac{\langle \mu(0) \bullet \mu(r) \rangle}{\langle \mu(0) \bullet \mu(0) \rangle} \qquad (3)$$

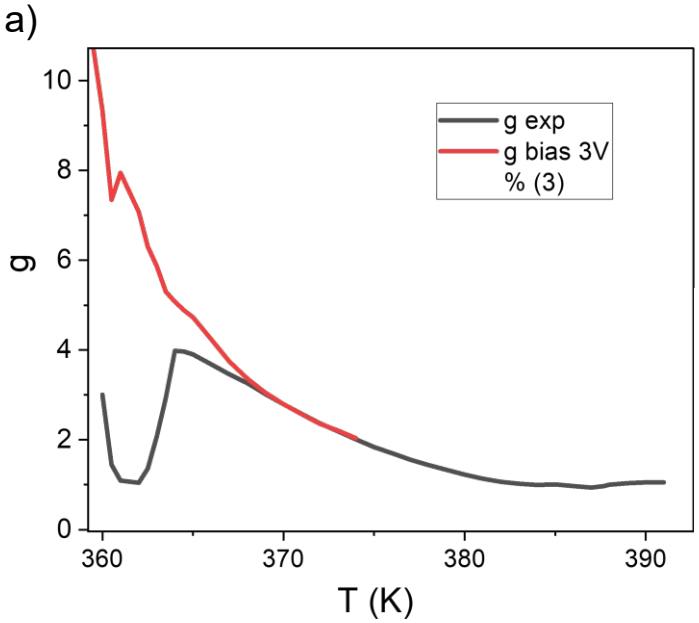

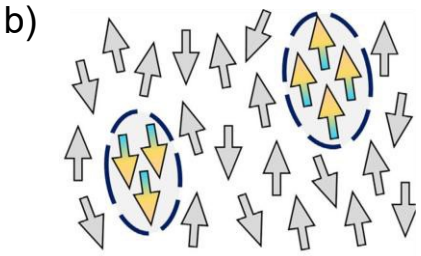

Fig. 4. a) Temperature dependence of Kirkwood coefficient, g, for 3JK, determined experimentally from dielectric spectroscopy: no biasing - black-solid line, with biasing 3 V- red-solid line,
b) Relaxor-Like Nature in Polar Nematic LC [28]

In MD, the local Kirkwood correlation factor, g, is calculated according to the classical definition from dielectric theory:

View Article Online
DOI: 10.1039/D6CP00046K

$$g_i = \frac{\left|\sum_{i=1}^{N} \vec{\mu}_i\right|^2}{N\left\langle \mu^2 \right\rangle} \quad (4)$$

where: $\vec{\mu}$ - the dipole moment vector of the i_{th} molecule, N -the number of molecules in the group, $\left\langle \mu^2 \right\rangle$ - the mean square value of the dipole moment magnitude in this group.

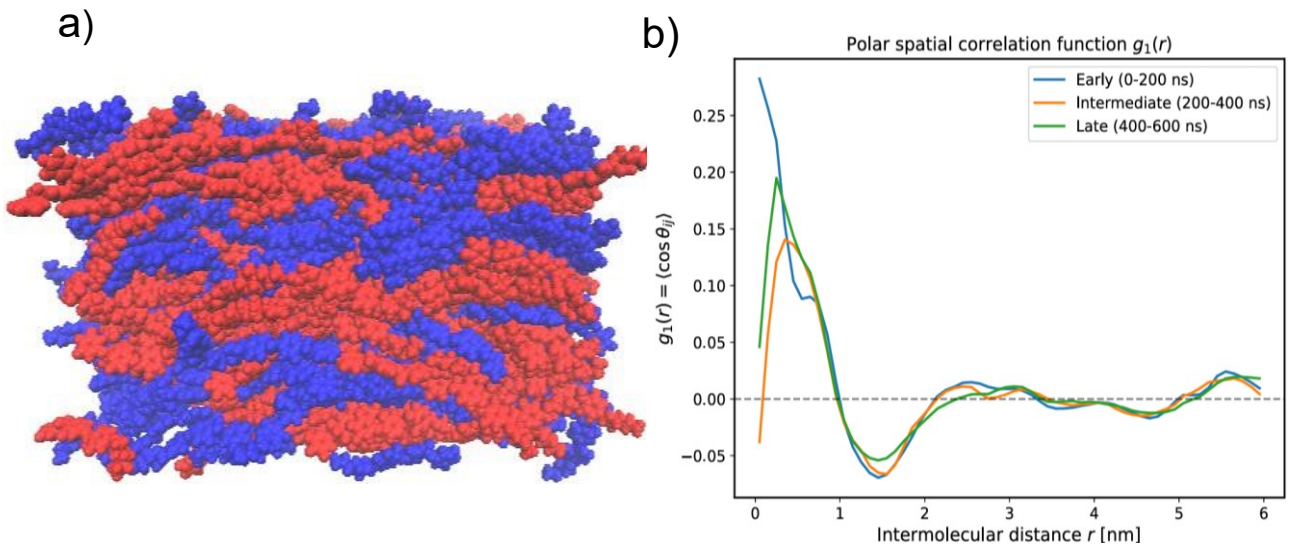

Figure 5. a) 3D visualization of the molecular arrangement in the polar nematic phase at 370 K. By coloring the molecules based on their projection along the local director axis, the presence of distinct nanodomains of opposite polar sense (e.g., red vs. blue regions) separated by clear domain walls is visually undeniable, **b)** distance-dependent polar spatial correlation function, *g1(r)*.

To provide clearer spatial evidence of domains with opposite polar sense, we have performed the requested analyses and added them to the manuscript and SI:

- **Images of the MD trajectory:** We have included 3D visual renders of the MD trajectory. By coloring the molecules based on their projection along the local director axis, the presence of distinct nanodomains of opposite polar sense (e.g., red vs. blue regions) can be observed.
- **Domain growth vs. simulation time:** We have generated 2D spatial polarization maps (heatmaps) tracking the evolution of the domains across the simulation timeline (Early, Intermediate, and Late stages). These maps show that the polar domains grow, consolidate, and stabilize over time, indicating they are a thermodynamic feature of the phase rather than a transient artifact of the initial conditions (Fig. S3).
- **Spatial correlation of P1:** We calculated the distance-dependent polar spatial correlation function, g1(r). As shown in the newly added Figure, g1(r) exhibits a positive correlation at short distances (parallel alignment within a domain) but systematically decays and crosses zero, reaching negative values at intermolecular distances of approximately 1.5 nm. This negative correlation provides quantitative evidence that

View Article Online
DOI: 10.1039/D6CP00046K

molecules at this distance possess an opposite polar sense, supporting the visual and mapping data of the nanodomain

This observation suggests that specific intermolecular interactions, rather than just a mean-field dielectric effect, are responsible for the observed spectral features [27, 28, 35]. The strong coupling between vibrations of neighboring molecules modifies the transition dipole moments, leading to the observed average intensity changes. For a given band, the average absorbance (A_0) should be proportional to the density. However, experimentally, Fig. 3b), A_0 drops significantly at the transition from isotropic to N phase and remains below extrapolated predictions with decreasing temperature. In N_F phase intensities of parallel band increase substantially but decrease for perpendicular bands. In fact, dielectric spectroscopy also shows that self-assembling gradually grows already in the nematic phase. This anomalous behavior, previously observed in the N-N_{TB} transition [35-37], confirms that specific molecular self-assembly and dipole-dipole correlations are dominant factors [39, 40].

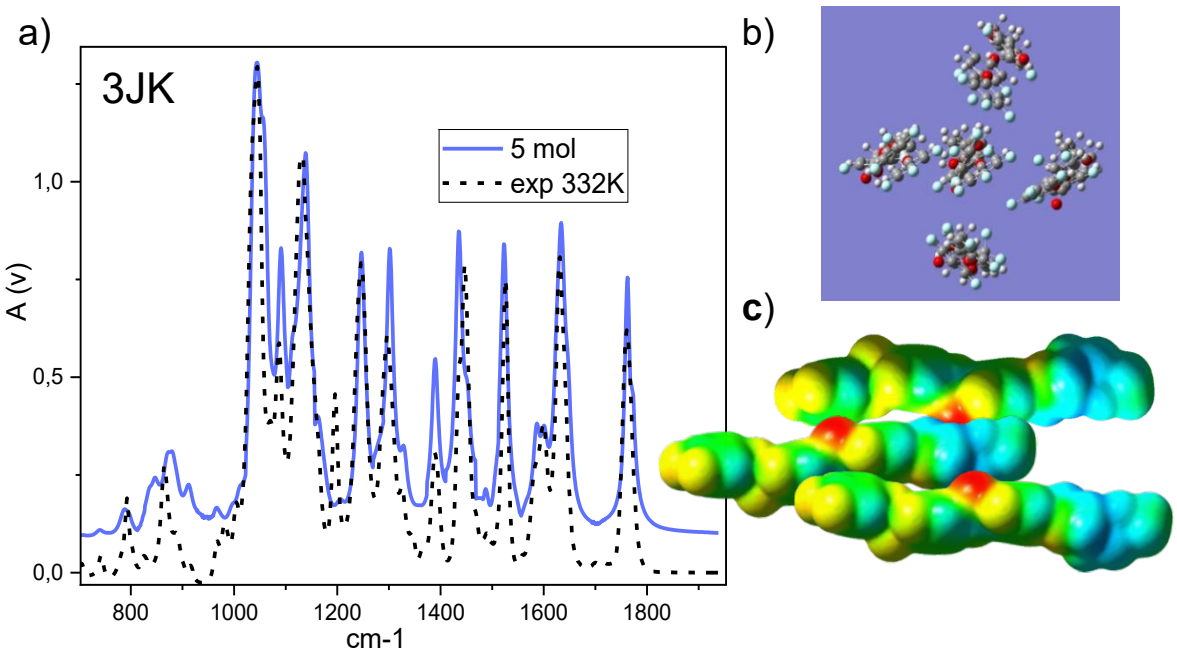

Figure 6. a) The comparison of the DFT simulated spectra of the 3JK molecule (B3-LYP/6-311G+ (d,p)) in the local molecular environment (for representative domain) with experimental spectrum (332 K): DFT simulated spectra of 3JK molecule as a result of vibrations coupling-blue solid line, experimental spectra - black dash line **b)** molecules arrangement in the domain-top view, **c**) side view of the molecular arrangements with electrostatic iso-potential surface. Please note the parallel molecular orientation and relative shift with respect to each other along the long axis.

To investigate the influence of neighboring molecules on the IR spectrum within a more realistic environment [38-40], we performed atomistic molecular dynamics (MD) simulations of 3JK molecules. Typical snapshots of the domains were selected at a temperature of 360 K, and DFT optimizations were carried out for a configuration consisting of five molecules. The

View Article Online
DOI: 10.1039/D6CP00046K

IR spectrum calculated for this system (Fig.6) shows significantly better agreement with the experimental spectrum.

3.3. Orientational Order Parameters

The primary nematic order parameter, *S*, was determined from the dichroism of several parallel vibrational bands (e.g., phenyl stretching at 1080, 1260, and 1525 cm^{-1}).

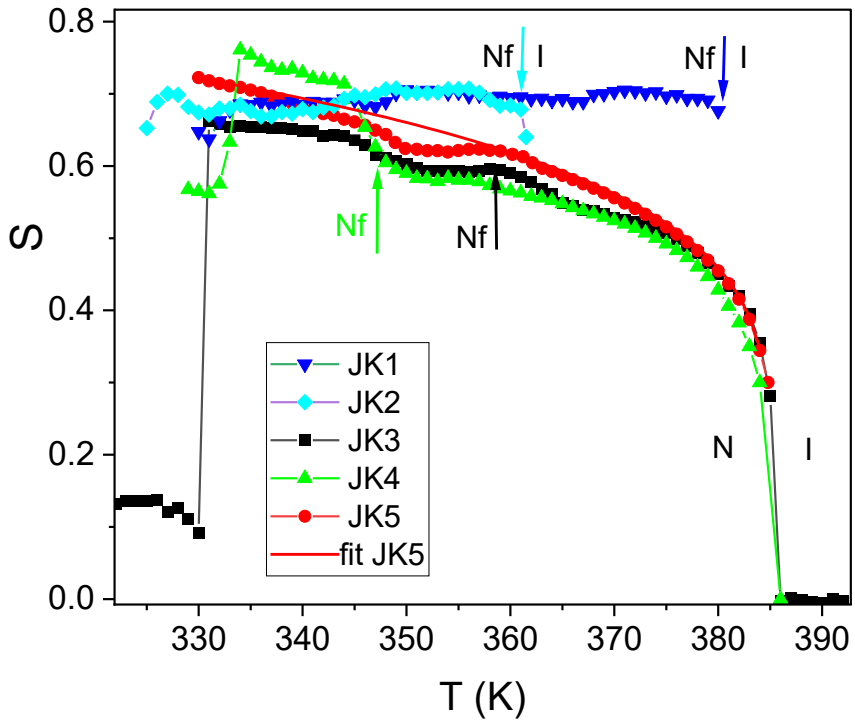

Fig.7. Temperature dependence of *S*-order parameters calculated for all nJK series, determined from 1525 cm^{-1} band absorbance. Fitting the power law eqn to the data 5JK. Symbols: -▼-, -◆-, -■-, -▲-, -●-, -are for n = 1, 2, 3, 4 and 5 respectively.

Figure 7 shows the temperature dependence of *S* for the nJK series. In the conventional nematic (N) phase, *S* exhibits a typical temperature dependence, which can be fitted with a power law with a critical exponent of 0.205 ± 0.005. This are rather typical as for other system DIO-like molecules [7, 11]. Anomalous departures from this behavior are observed at the N-N_X and N_X-N_F phase transitions. Upon entering the N_F phase, *S* reaches a high value of approximately 0.7 and remains nearly constant for 1JK and 2JK.

We believe that the orientational order parameter depends mainly on the local molecular arrangement. Experimental results do not show significant changes at the phase transitions (N, N_X, and N_F) within the nematic phase range, unlike other quantities such as permittivity or polarization. The overall temperature behavior of the orientational order parameters in the range of nematic subphases are mainly determined by temperature difference T_{NI}-T. Typical behavior is shown for 5JK molecule, that have only nematic phase, ***S***-parameter is changing from **0.3 to 0.72** in nematic phase as usually for majority of nematic LC. For 3JK and 4JK, in the nematic phase, *S* parameters follow the similar way as for 5JK, but decline slightly on entering N_X, and N_F probably due to different packing higher molecular flexibility and escaping from uniform

alignment. The Iso–N_F (Isotropic to Ferroelectric Nematic) phase transition for 1JK and 2JK homologues is a first-order phase transition characterized by a discontinuous, abrupt change in the order parameter. A defining feature of this transition is a discontinuous jump in the order parameter S at the transition temperature (T_C) [41]. Unlike the conventional isotropic-nematic (I-N) transition, which is usually only weakly first-order, the direct transition to the ferroelectric nematic (N_F) phase involves a significant jump in both orientational order S and electric polarization P.

The order parameters were calculated using a custom Python script utilizing the MD Analysis library. The nematic order parameter, P_2 was determined by diagonalizing the Saupe ordering tensor, Q, constructed from the molecular long axes (defined as the principal axis of the smallest moment of inertia). The phase director, n, corresponds to the principal eigenvector of Q. The polar order parameter P_1 was calculated as the ensemble average of the projection of the normalized molecular dipole moment vectors onto the phase director, n. We have significantly expanded the relevant paragraph in the *Methods* section to provide these mathematical details.

These results are in qualitative agreement with the predictions from our atomistic simulations for 3JK (Fig. S2). Ferroelectric ordering was found to be present at 340 K in the simulation system 3JK. As a result of applying the field of 0.05V/nm, the polar order parameter approach P_1=0.82.

3.4. Phase Biaxiality

A key finding of this study is the significant difference observed between the A_X and A_Y absorbance components for perpendicular vibrations (e.g., at 870 cm^{-1} and 1760 cm^{-1}).

According to the theoretical framework, the difference (A_Y-A_X) is a direct experimental signature of phase biaxiality, related to the parameters P and C. We define an "apparent biaxiality" parameter as (A_Y-A_X)/A_0. Following eq.(2) the apparent biaxiality can be related to Saupe order parameters:

$$(A_Y - A_X)/A_0 = P(3\sin^2\beta - 2) + C\sin^2\beta\cos 2\phi \qquad (5)$$

Figure 7 shows that this apparent biaxiality is non-zero and increases significantly upon cooling through the nematic range, reaching values up to 0.4 in the N_F phase. Since the perpendicular components of parallel vibrations do not show significant difference ($A_X \approx A_Y$), we attribute this biaxiality primarily to the ordering of the secondary director (parameter C), in the second part in eq.(5). Application of a 1T magnetic field further increases the measured biaxiality, confirming that it is related to the macroscopic alignment of the secondary director.

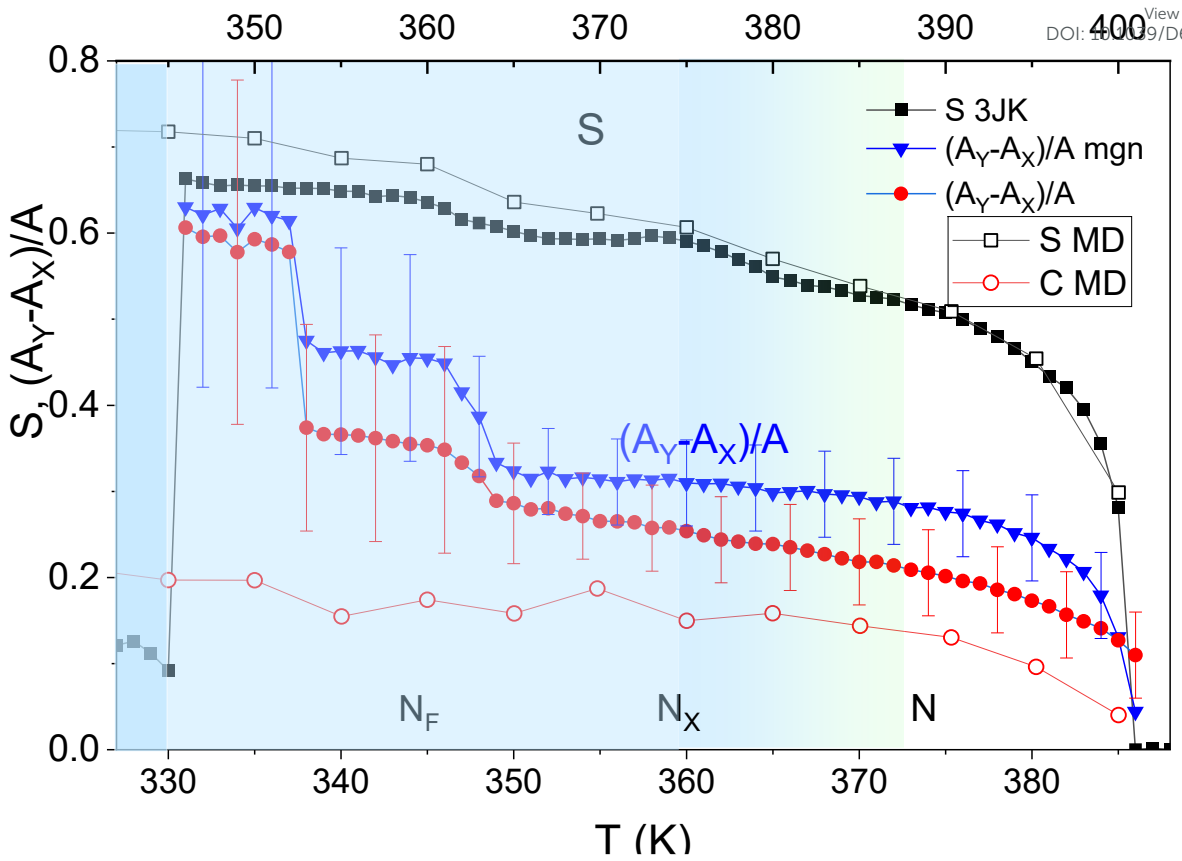

Fig. 8. Temperature dependence of *S*-order parameters for 3JK, -■-, and biaxiality of the phase $(A_Y\text{-}A_X)/A_0$ calculated for 3JK, determined from 1760 cm^{-1} band absorbance without: -■- , and in the magnetic field (B=1T), -▼-. Molecular dynamic prediction for *S* parameter, *S*: -□-, and phase biaxiality -○-.Please note, the upper scale for MD results is shifted by15K with respect to the bottom one.

After accounting for the angular factors in Eq. 5, the real biaxiality order parameter (*C*) expect to be probably higher than $(A_Y\text{-}A_X)/A_0$, indicating a significant biaxial ordering. The experimentally derived apparent biaxiality, $(A_Y\text{-}A_X)/A_0$ has two terms, eq.(5), which are difficult to separate, It has to be noted that biaxiality, *C*-parameter, from atomistic simulations are substantially lower than experimental apparent one, $(A_Y\text{-}A_X)/A_0$ thus the difference can be due to the first term in eq (5) which may also have significant contribution due to the splay deformations. We believe that biaxiality has a significant impact on the electrical response of the system.

For a complex molecule like 3JK, several key interactions are typically neglected or oversimplified in classical MD simulations. "In the case of 3JK accurately modeling short-range interactions is crucial. While standard MD captures dipole-dipole interactions, it may overlook molecular polarizability and the specific electronic distribution of the groups. The most significant limitation for 3JK in standard MD is the lack of polarizability. Since the polar DIO phase involves massive local internal fields that "pump" the molecular dipoles, a non-polarizable model may yield an orientational order parameter that is lower than what you observe in IR or birefringence experiments.

What is omitted:

View Article Online
DOI: 10.1039/D6CP00046K

The redistribution of the electron cloud under the influence of the intense local electric fields found in the ferroelectric-like (DIO) phase. For a highly fluorinated molecule like 3JK, the induced dipoles can significantly strengthen intermolecular coupling, a factor the classical model cannot see.

The subtle quantum mechanical effects of π orbital overlapping. These effects dictate whether the aromatic rings align "face-to-face" or "edge-to-face," which is critical for determining the orientational order parameter in nematic phases.

While fluorine is a weak halogen bond donor, in such highly substituted systems, MD typically misses the anisotropy of these interactions, which helps stabilize local molecular packing.

The coupling between the molecule's conformational state and the local dielectric environment. In reality, a change in conformation alters the molecular dipole moment. In dielectric spectroscopy, this is a primary signal, but in fixed-charge MD, this effect is often significantly underestimated.

IV. Conclusions

In this work, we employed polarized FTIR spectroscopy, complemented by DFT calculations and atomistic simulations, to investigate the molecular organization in polar nematic phases of the JKn homologous series. Our key findings are as follows:

1. **Intermolecular interactions are dominant:** Simple DFT models of isolated molecules are insufficient to describe the vibrational spectra of these materials. The anomalous temperature dependence of the average absorbance indicates that specific short-range molecular correlations, rather than mean-field effects, govern the system's properties. Atomistic simulations support this conclusion by revealing the formation of locally ordered nanodomains.
2. **Quantification of orientational order:** The primary order parameter, *S*, shows distinct behavior across the N, N_X, and N_F phases, reaching a high saturation value of $S \approx 0.7$ in the ferroelectric state.
3. **Evidence of the phase biaxiality:** A significant difference between the A_X and A_Y absorbance components for perpendicular vibrations was observed, providing direct evidence of macroscopic phase biaxiality. This biaxiality increases upon cooling and is particularly pronounced in the N_F phase, where the secondary order parameter C exceeds value 1.0.

This combined experimental and theoretical approach highlights the complex interplay between molecular structure, local self-assembly, and the resulting macroscopic polar order in this fascinating new class of liquid crystals.

Acknowledgments:

Authors JK, BN & AK thank the National Science Centre for funding through the Grant No. 2022/45/B/ST5/04093 (JK, BN & AK) and 2024/53/B/ST5/03275 (PK).

We gratefully acknowledge Polish high-performance computing infrastructure PLGrid (HPC Center: ACK Cyfronet AGH) for providing computer facilities and support within computational grant no. PLG/2025/018039

V. References

1. M. Born, Über anisotrope Flüssigkeiten. Versuch einer Theorie der flüssigen Kristalle und des elektrischen Kerr-Effekts in Flüssigkeiten, *Sitzungsber. Preuss. Akad. Wiss.*, 1916, 30, 614–650.
2. R. J. Mandle, S. J. Cowling and J. W. Goodby, Rational design of rod-like liquid crystals exhibiting two nematic phases, *Chem. Eur. J.*, 2017, 23, 14554–14562.
3. H. Nishikawa, K. Shiroshita, H. Higuchi, et al., A fluid liquid-crystal material with highly polar order, *Adv. Mater.*, 2017, 29, 1702354.
4. X. Chen, E. Korblova, D. Dong, et al., First-principles experimental demonstration of ferroelectricity in a thermotropic nematic liquid crystal: polar domains and striking electro-optics, *Proc. Natl. Acad. Sci. U. S. A.*, 2020, 117, 14021–14031.
5. H. Nishikawa, K. Sano, S. Kurihara, et al., Nano-clustering mediates phase transitions in a diastereomerically-stabilized ferroelectric nematic system, *Commun. Mater.*, 2022, 3, 89.
6. X. Chen, E. Korblova, M. A. Glaser, et al., Polar in-plane surface orientation of a ferroelectric nematic liquid crystal: polar monodomains and twisted state electro-optics, *Proc. Natl. Acad. Sci. U. S. A.*, 2021, 118, e2104092118.
7. N. Sebastián, L. Cmok, R. J. Mandle, et al., Ferroelectric-ferroelastic phase transition in a nematic liquid crystal, *Phys. Rev. Lett.*, 2020, 124, 037801.
8. C. L. Folcia, J. Ortega, R. Vidal, et al., The ferroelectric nematic phase: an optimum liquid crystal candidate for nonlinear optics, *Liq. Cryst.*, 2022, 49, 899–906.
9. J. Ortega, C. L. Folcia, J. Etxebarria, et al., Ferroelectric chiral nematic liquid crystals: new photonic materials with multiple bandgaps controllable by low electric fields, *Liq. Cryst.*, 2022, 49, 2128–2136.
10. D. Pociecha, R. Walker, E. Cruickshank, et al., Intrinsically chiral ferronematic liquid crystals: an inversion of the helical twist sense at the chiral nematic – chiral ferronematic phase transition, *J. Mol. Liq.*, 2022, 361, 119532.
11. J. Karcz, J. Herman, N. Rychłowicz, P. Kula, E. Gorecka, J. Szydlowska, P. W. Majewski and D. Pociecha, Ferroelectric nematic phase in achiral calamitic liquid crystals with a terminal cyano group, *Science*, 2024, 384, 1096–1100.
12. J. Li, H. Nishikawa, J. Kougo, et al., Development of ferroelectric nematic fluids with giant-ε dielectricity and nonlinear optical properties, *Sci. Adv.*, 2021, 7, eabf5047.
13. J. Li, Z. Wang, M. Deng, et al., General phase–structure relationship in polar rod-shaped liquid crystals: importance of shape anisotropy and dipolar strength, *Giant*, 2022, 11, 100109.
14. R. Saha, P. Nepal, C. Feng, et al., Multiple ferroelectric nematic phases of a highly polar liquid crystal compound, *Liq. Cryst.*, 2022, 49, 1784–1796.
15. J. Karcz, N. Rychłowicz, M. Czarnecka, A. Kocot, J. Herman and P. Kula, Enantiotropic ferroelectric nematic phase in a single compound, *Chem. Commun.*, 2023, 59, 14807–14810.
16. H. Nishikawa, K. Sano and F. Araoka, Anisotropic fluid with phototunable dielectric permittivity, *Nat. Commun.*, 2022, 13, 1142.
17. R. J. Mandle, N. Sebastián, J. Martinez-Perdiguero, et al., On the molecular origins of the ferroelectric splay nematic phase, *Nat. Commun.*, 2021, 12, 4962.
18. A. Manabe, M. Bremer and M. Kraska, Ferroelectric nematic phase at and below room temperature, *Liq. Cryst.*, 2021, 48, 1079–1086.
19. J. Li, R. Xia, H. Xu, et al., How far can we push the rigid oligomers/polymers toward ferroelectric nematic liquid crystals?, *J. Am. Chem. Soc.*, 2021, 143, 17857–17861.

20. N. Vaupotič, D. Pociecha, P. Rybak, et al., Dielectric response of a ferroelectric nematic liquid crystalline phase in thin cells, *Liq. Cryst.*, 2023, 50, 584–595.
21. E. B. Wilson, J. C. Decius and P. C. Cross, Molecular Vibrations, McGraw-Hill, New York, 1955.
22. P. G. de Gennes and J. Prost, The Physics of Liquid Crystals, Oxford University Press, Oxford, 2nd edn, 1993.
23. D. Dunmur and K. Toriyama, in Handbook of Liquid Crystals, ed. D. Demus, J. Goodby, G. W. Gray, H.-W. Spiess and V. Vill, Wiley-VCH, Weinheim, 2001, vol. 1A, ch. VII, pp. 189–281.
24. Gaussian 16, Revision C.01, M. J. Frisch, G. W. Trucks, H. B. Schlegel, et al., Gaussian, Inc., Wallingford CT, 2019.
25. N. J. Boyd and M. R. Wilson, Optimization of the GAFF force field to describe liquid crystal molecules: the path to a dramatic improvement in transition temperature predictions, *Phys. Chem. Chem. Phys.*, 2015, 17, 24851–24865.
26. G. Bussi, D. Donadio and M. Parrinello, Canonical sampling through velocity rescaling, *J. Chem. Phys.*, 2007, 126, 014101.
27. M. J. Abraham, T. Murtola, R. Schulz, et al., GROMACS: High performance molecular simulations through multi-level parallelism from laptops to supercomputers, *SoftwareX*, 2015, 1, 19-25.
28. F. Ye, Y. Hou, C. Yang, et al., Intrinsic Relaxor-Like Nature in Single-component Polar Nematic Fluids, *Small*, 2026, 0, e12407.
29. J. Wang, R. M. Wolf, J. W. Caldwell, P. A. Kollman and D. A. Case, Development and testing of a general amber force field, *J. Comput. Chem.*, 2004, 25, 1157-1174.
30. A. W. Sousa da Silva and W. F. Vranken, ACPYPE - AnteChamber PYthon Parser interfacE, *BMC Res. Notes*, 2012, 5, 367.
31. M. Parrinello and A. Rahman, Polymorphic transitions in single crystals: A new molecular dynamics method, *J. Appl. Phys.*, 1981, 52, 7182.
32. N. Michaud-Agrawal, E. J. Denning, T. B. Woolf and O. Beckstein, MDAnalysis: A toolkit for the analysis of molecular dynamics simulations, *J. Comput. Chem.*, 2011, 32, 2319-2327.
33. R. J. Gowers, M. Linke, J. Barnoud, et al., MDAnalysis: A Python package for the rapid analysis of molecular dynamics simulations, *Proc. 15th Python Sci. Conf.*, 2016, 98-105.
34. U. Essmann, L. Perera, M. L. Berkowitz, T. Darden, H. Lee and L. G. Pedersen, A smooth particle mesh Ewald method, *J. Chem. Phys.*, 1995, 103, 8577.
35. K. Merkel, B. Loska, C. Welch, G. H. Mehl and A. Kocot, The role of intermolecular interactions in stabilizing the structure of the nematic twist-bend phase, *RSC Adv.*, 2021, 11, 2917–2924.
36. A. Kocot, M. Czarnecka, Y. Arakawa and K. Merkel, Exploring the impact of intermolecular interactions on the glassy phase formation of twist-bend liquid crystal dimers: insights from dielectric studies, *Molecules*, 2023, 28, 7441.
37. A. Kocot, B. Loska, Y. Arakawa and K. Merkel, Structure of the twist-bend nematic phase with respect to the orientational molecular order of the thioether-linked dimers, *Phys. Rev. E*, 2022, 105, 044701.
38. A. Wiedenmann, A. Hoell, M. Kammel and P. Boesecke, Field-induced pseudocrystalline ordering in concentrated ferrofluids, *Phys. Rev. E*, 2003, 68, 031203.
39. A. A. Marchenko, O. L. Kapitanchuk, Y. Yu, et al., Polar Self-Organization of Ferroelectric Nematic-Liquid-Crystal Molecules on Atomically Flat Au(111) Surface, *Phys. Rev. Lett.*, 2024, 132, 098101.
40. N. V. Madhusudana, Simple molecular model for ferroelectric nematic liquid crystals exhibited by small rodlike mesogens, *Phys. Rev. E*, 2021, 104, 014704.
41. J. Szydlowska, P. Majewski, M. Čepič, et al., Ferroelectric Nematic-Isotropic Liquid Critical End Point, *Phys. Rev. Lett.*, 2023, 130, 216802.

View Article Online
DOI: 10.1039/D6CP00046K

Data sharing and long-term preservation

The data will be archived in the digital archiving system of the University of Silesia (ZENODO) and the Repository of the Jagiellonian University (RUJ). The ZENODO University of Silesia Repository will allow storing and sharing full publications, while RUJ will allow storing raw research data. The Jagiellonian University repository meets the FAIR

Data principles, which in its development mean: (Findable, Accessible, Interoperable, Reusable). All data are openly available at the end of this project.

The raw data, as a result of direct measurements, will include FTIR and Raman spectra, which will be converted to the "txt" or "csv" file as a universal framework and will be deposited in the RUJ database. Raw data from computer simulations will be converted to the "txt" or "log" text files and will also be deposited in RUJ.https://zenodo.org/ https://ruj.uj.edu.pl/xmlui/

The data will be made publicly available when research results are published and / or any intellectual property of the site generated under this research project is sufficiently protected. All data stored on the RUJ will have a DOI number, will be described: project name, data of the introductory person and project manager, date of project duration. ZENODO will be the main platform for data storage. Data provided in the Repository will fulfill FAIR standards requirements and will be categorized and labeled according to the standard file formats. There is no time limit for data storage at ZENODO.

Digital Commons and RUJ/ZENODO databases are fully public and searchable via any web browser. The data will be stored for the duration of the project.